Chemical Engineering Science 265 (2023) 118226

Contents lists available at ScienceDirect

Chemical Engineering Science

journal homepage: www.elsevier.com/locate/ces

A numerical investigation of the hydrodynamic and mass transfer behavior of a liquid-liquid semi-partition bioreactor (SPB) designed for *in-situ* extractive fermentation

George M. Teke [a], Godfrey K. Gakingo [a,b], Robert W.M. Pott [a,*]

[a] Department of Process Engineering, Stellenbosch University, South Africa
[b] Department of Chemical Engineering, Dedan Kimathi University of Technology, Kenya

HIGHLIGHTS

- A CFD model for a multiphase semi-partition bioreactor (SPB) is developed.
- The hydrodynamics and mass transfer within the multiphase SPB are investigated.
- Results show need for minimum agitation speed for homogeneity in mixer section of SPB.
- Results affirm the SPB works by liquid-liquid partitioning, phase separation and extraction.

ARTICLE INFO

Article history:
Received 23 July 2022
Received in revised form 27 September 2022
Accepted 13 October 2022
Available online 20 October 2022

Keywords:
Extractive fermentation
Semi-partition bioreactor
Liquid-liquid extraction
Mass transfer
Hydrodynamics
Computational fluid dynamics (CFD)

ABSTRACT

Organisms used in fermentation processes are sometimes inhibited by accumulation of products or by-products. One route to circumvent this is via extractive fermentation. To facilitate this, novel bioreactor designs are required, such as the semi-partition bioreactor (SPB) which has been designed for *in-situ* extractive fermentation. This study reports on the numerical investigation of an SPB, considering phase separation, hydrodynamics and mass transfer behaviour. Key findings illustrate that a minimum agitation speed is necessary to attain system homogeneity in the mixer section. Furthermore, the results indicate that the working principle of the bioreactor will be effective for liquid-liquid partitioning and mass transfer followed by flux exchange between the mixer and settler sections and subsequent phase separation in the settler section. This mechanism has a shorter characteristic time than the replenishment of the bioreactor with recycled (and back-extracted) extractant. The reactor thus shows promise as a route for fermentations susceptible to product inhibition.

1. Introduction

Industrial microbial fermentation involves the use of organisms (for instance bacteria, fungi or algae) to produce various products (such as fuels, solvents, proteins, fragrance, flavours or organic acids) in several industries (such as the food, cosmetic, fine chemicals, agriculture, biotechnology and pharmaceuticals sectors). Although the use of such organisms has been shown to have significant potential, production using organisms can be inhibited due to accumulation of products or by-products that are toxic to the organisms at high enough concentrations (Wang, 1983). Over the years, product accumulation has been avoided via improved biological strains, through genetic engineering, by optimizing bioreactor configurations or through extractive fermentation (Kuila and Sharma, 2018; Stanbury et al., 2017; Stark and von Stockar, 2003; Teke et al., 2021). Extractive fermentation in particular has been seen as an effective route, not only in increasing yield and productivity due to reduced inhibition, but also aiding in the reduction of the overall number of processing steps that occur further downstream (Van Hecke et al., 2014; Stark and von Stockar, 2003).

Extractive fermentation involves a traditional fermentation unit combined with separation vessels operating on one or more of the known separation principles (gas-stripping, pervaporation, electrodialysis, adsorption, precipitation or liquid–liquid extraction) (Stark and von Stockar, 2003). Teke et al. (2021) have given a recent overview of this topic, highlighting that extractive fermentation is essentially governed by gas–liquid, solid–liquid and liquid–liquid extraction principles. In the case of liquid–liquid

* Corresponding author.
E-mail address: rpott@sun.ac.za (R.W.M. Pott).

https://doi.org/10.1016/j.ces.2022.118226
0009-2509/

Nomenclature

D	Diameter of impeller (m)
$\vec{g}$	Acceleration due to gravity (9.81 m/s^2)
H	Tank height (m)
N	Rotational speed of the impeller (s^{-1})
d_p	droplet diameter (m)
T	Tank Diameter (m)

Greek letters

ε	turbulent kinetic energy dissipation rate (W/kg)
ρ	Density (kg/m^3)
μ_t	Viscosity of fluid (Pa.s)
$\bar{\tau}_q$	Turbulent stress tensor
λ_q	bulk viscosity of phase
D_i	Molecular diffusivity of product in ith phase (m^2/s)
v	kinematic viscosity (m^2/s)

Subscripts & superscripts

q	continuous aqueous phase
p	dispersed organic phase

Abbreviations

SPB	Semi partition bioreactor
MRF	Multiple reference frame
rpm	Rotations per minute
K_La	overall mass transfer coefficient

extraction, which is of interest to this study, a secondary dispersed liquid (usually a solvent, ionic liquid, or an emergent second phase) is added to the fermentation set-up internally. This results in a multiphase set-up in which the micro-organisms reside in the continuous aqueous phase while the secondary dispersed liquid phase acts as a sink and reservoir for inhibitory product(s) or by-product (s). As the added dispersed phase can be removed from the fermentation vessel, the products held within back-extracted and the solvent recycled, the concept of liquid–liquid extraction becomes attractive for use in commercial bioprocesses. However, the presence of the secondary liquid phase makes the system complex with regards to its hydrodynamics and mass transfer behaviour. Thus, the changes in hydrodynamics and mass transfer behaviour need to be investigated to establish standards for design of novel liquid–liquid extractive fermentation systems.

Recently, a novel semi-partitioned bioreactor (SPB) has been proposed for use in liquid–liquid extraction of inhibitory products (James et al., 2021; Teke, 2019; Teke et al., 2022a; Teke and Pott, 2021). The design concept of the SPB is to function as a single unit consisting of both a mixer and a settler section. The former permits the production of a sample product in one phase (primary phase) and its transfer from the primary phase to a secondary, immiscible, phase which is removed via the settler section of the SPB. The settler thus acts as a dead zone where the secondary phase separates from the primary phase thereby permitting continuous solvent removal and product extraction.

The behaviour of the proposed SPB has so far been investigated through experimental mixing studies and numerical hydrodynamic and mass transfer studies (Teke et al., 2022a; Teke and Pott, 2021). For the latter, single-phase Computational Fluid Dynamics (CFD) models were used to generate some insights into the system's hydrodynamics and mass transfer behaviour. Such insights included the observation that the convective flux between/across the mixer and settler sections of the SPB was time-dependent and that its approximation using constant values led to inaccurate predictions of the mixing time in the SPB (Teke et al., 2022a). This observation was only captured based on investigations using the CFD models, highlighting the need to use such comprehensive models as opposed to simple mathematical models (Teke et al., 2022a). Also, the single-phase results demonstrated several changes in flow patterns from a traditional stirred tank system due to the addition of the settler inserted tube, while proposing possible spots for a potential inter-compartment position relocation (Teke et al., 2022a).

Though such insights were useful, it must be acknowledged that a realistic SPB working on liquid–liquid extraction principles will involve multiple phases including at least two liquid phases as well as a solid phase (the micro-organisms). Thus, the hydrodynamics are expected to be more complex. There is, therefore, a need to extend the single-phase CFD model previously developed to account for multiple phases and to use this extended model in the comprehensive study of the hydrodynamics and mass transfer behaviour of realistic SPB systems.

This article demonstrates, for the first time, the development of a two-phase liquid–liquid CFD model for an SPB and utilizes the latter to generate insights on the operating principles of the novel design. The model has been validated against experimental investigations into phase separation with and without liquid–liquid extraction. Finally, the model has been used to study the hydrodynamic and mass transfer behaviour of the SPB under various values of the volumetric removal rate. Insights on the operation of the SPB have been generated, such as the minimum agitation speed needed for system homogeneity, and such insights are expected to be useful to biochemical engineers seeking to propose, build and operate similar reactors.

2. Methodology

2.1. Materials

n-hexane was purchased from Sigma Aldrich with a 97 % purity, Red Oil O dye was supplied from Merck and deionized water was obtained from the laboratory. The numerical simulation employed water and *n*-hexane with density and viscosity properties (from Michailidou et al., 2013) shown in Table 1.

2.2. Set-up

Similar to previous studies (Teke et al., 2022a; Teke et al., 2022b; Teke and Pott, 2021), a 5 L working volume stirred tank (180 mm diameter) fitted with baffles was used with two six-bladed standard Rushton turbine impellers (60 mm diameter) employed to generate agitation at different speeds (200, 300 and 450 rpm). This formed the mixer section of the SPB (see Fig. 1). A 40 mm diameter glass tube with a side opening (35 mm diameter) was inserted into the tank to form the settler section. Water and *n*-

Table 1
Fluid physical properties of components.

	Density ($\frac{kg}{m^3}$)	Viscosity (mPa.s)
Water	998.00	1.00
n-hexane	655.00	0.30

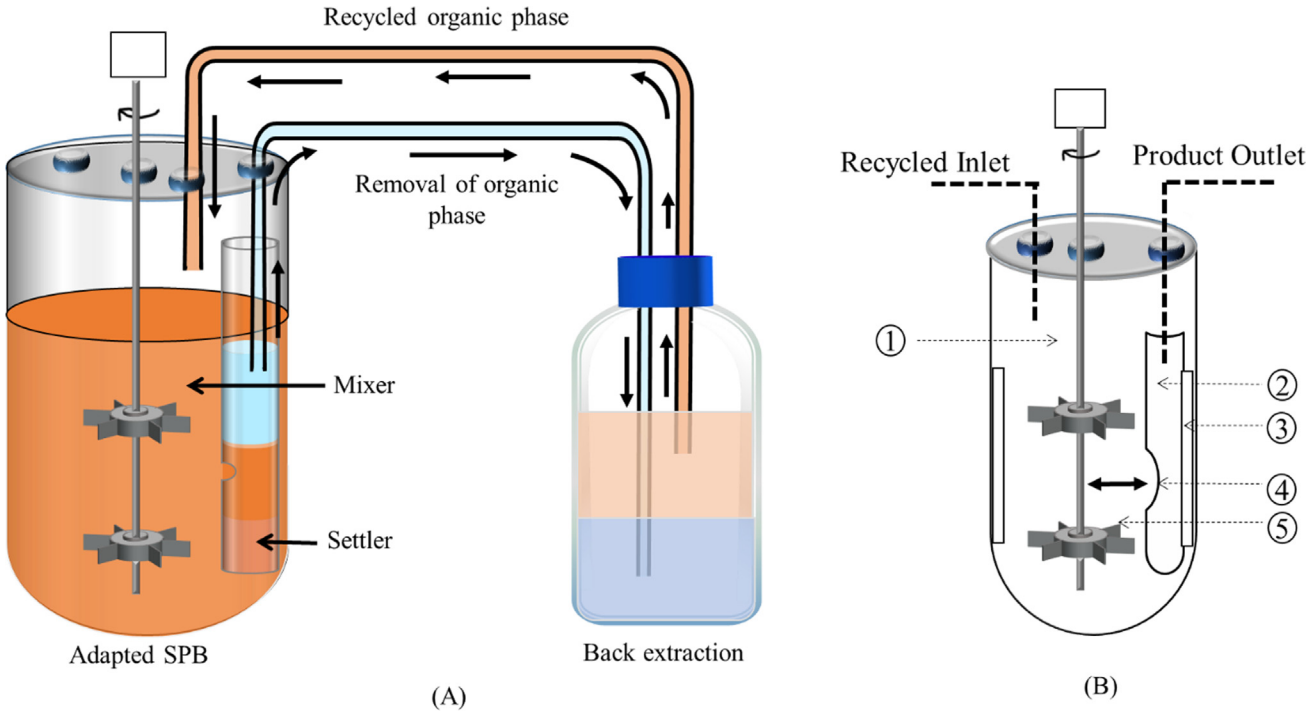

Fig. 1. Schematic for liquid–liquid extractive fermentation through a semi-partition bioreactor (SPB). (A) Full experimental setup and (B) the bioreactor. (1) mixer, (2) settler, (3) baffles, (4) intercompartmental space (permits movement of fluids) and (5) Rushton turbine impellers.

hexane were used in this study, with the continuous aqueous phase being water and the dispersed organic phase being *n*-hexane. The concentration of the latter was 10 % by volume, gotten from a previous study and from literature (Teke and Pott, 2021; Yabannavar and Wang, 1991).

As shown in Fig. 1A, the mixer section was used to produce the product which was then absorbed by the dispersed organic phase. In the settler, the rich organic phase settled out and was removed to a back extraction unit for stripping (product removal from the organic phase). Finally, the stripped organic phase was returned to the mixer section (recycled).

2.3. Experimental measurement procedures

Phase separation in the settler section is needed for successful extractive fermentation in an SPB. It is the design of the SPB that immiscible phases contacting in the mixer section should be able to rapidly separate in the settler section so as to allow continuous extraction of the top-phase which should be rich in the bioproduct of interest. Hence, the phase separation behaviour of the SPB is investigated in this section.

2.3.1. Phase separation measurements (without top-phase extraction)

The SPB system was filled with *n*-hexane and water in a ratio of 1:9. The two phases were visually differentiated by adding 1 ml Red Oil O dye which preferentially partitions to the organic phase. At the start of the experiment, no organic phase was present in the settler section of the SPB. However, with continuous mixing, some of the organic phase got introduced into the settler column and settled out as a top phase due to the quiescent conditions within this column. After sufficient time was allowed for the attainment of steady-state (30 min of mixing), the details of phase separation were captured with a digital camera (iPhone 12 Pro model – with a resolution of 1170 × 2532 pixels and ~ 460 ppi) to provide qualitative analysis. The height of the settled organic phase (in the settler section) was also measured and converted to a volume based on the pre-determined diameter of the settler column. Such measurements provided quantitative values at different agitation speeds (200, 300 and 450 rpms) to compare against CFD predictions.

2.3.2. Phase separation measurements (with top-phase extraction)

These experiments were similar to those above in that phase separation was allowed to occur after introducing *n*-hexane and water into the SPB. However, in this case, continuous removal of the organic phase that had settled out in the settler column occurred (removal of top-phase). This was done at different volumetric removal rates (1, 5, 15, 30, 60, 150, and 300 ml/min), with the organic phase recycled into the mixer section at the same rate as the removal rates so as to maintain a constant volume of the organic phase during operation. The agitation rate was kept at 300 rpm for these experiments as it achieved sufficient homogeneity and phase dispersion in the mixer (see Results).

After running the SPB in the above manner for an hour to acquire system stability, the height of the organic phase that had settled out in the settler column was measured. This value was converted into a volume based on the diameter of the SPB. Such values provided quantitative measurements at different volumetric flow rates to compare against CFD predictions.

2.3.3. Viscosity measurement

Lactic acid bacteria (*Lactobacillus casei*) were grown in a 250 ml Erlenmeyer flask at 37 °C for 24 h (Teke et al., 2022b; Teke, 2022). The optical density (OD) of the cells (biomass) at 620 nm was obtained with the help of a UV/VIS spectrophotometer. The biomass concentration (in g/L) was then estimated using an OD versus CDW (Cell dry weight) calibration curve.

The viscosity of the estimated biomass concentration (in g/L) was then determined using an Anton Paar (Physica MCR 50) rheometer with a concentric cylinder measuring system (CC27). The rotating measurements were obtained at temperatures of 25 °C and 37 °C. These measurements were done in triplicate.

2.4. Numerical simulation

2.4.1. Model description (hydrodynamics)

The governing equations of single-phase flow, as shown in a previous study (Teke et al., 2022a), were extended to the two-phase liquid–liquid system based on a standard formulation – the Eulerian-Eulerian two-fluid model. This model has been used in previous CFD studies involving stirred tank systems (Cheng et al., 2013; Laurenzi et al., 2009; Wang and Mao, 2005; Weber et al., 2020) and treats the phases as interpenetrating continua with the sum of their volume fractions equal to unity (see equation (1) below with subscripts q and p referring to the continuous aqueous phase and the dispersed organic phase respectively). The governing equations of flow could be written out as illustrated in equation (2) (continuity) and equation (3) (momentum) for the continuous phase, with similar equations for the dispersed organic phase.

$$\alpha_p + \alpha_q = 1 \tag{1}$$

$$\frac{\partial}{\partial t}\left(\alpha_q \rho_q\right) + \nabla \cdot \left(\alpha_q \rho_q \overrightarrow{V_q}\right) = 0 \tag{2}$$

$$\frac{\partial}{\partial t}\left(\alpha_q \rho_q \overrightarrow{V}_q\right) + \nabla \cdot \left(\alpha_q \rho_q \overrightarrow{V_q} \otimes \overrightarrow{V_q}\right) = -\alpha_q \nabla p + \alpha_q \rho_q \overrightarrow{g} + \nabla \cdot \bar{\bar{\tau}}_q + \overrightarrow{F}_q + \sum_{p=1}^{n} \overrightarrow{R}_{pq} \tag{3}$$

$$\bar{\bar{\tau}}_q = \alpha_q\left(\mu_q + \mu_{t,m}\right)\left(\nabla \overrightarrow{V}_q + \nabla \overrightarrow{V_q}^T\right) - \frac{2}{3}\alpha_q\left(\left(\mu_q + \mu_{t,m}\right)\nabla \cdot \overrightarrow{V_q} + \rho_q k\right)\bar{\bar{?}} \tag{4}$$

In the equations above, the density, mean velocity vector and volume fraction of the continuous phase (phase q) were represented by ρ_q, $\overrightarrow{V}_q$ and α_q respectively. The variable p represented the shared pressure of the phases whereas $\overrightarrow{g}$ represented the acceleration due to gravity. The variable $\bar{\bar{\tau}}_q$ represented the stress tensor (see equation (4)) in which both viscous and turbulent contributions of the motion were accounted for (flow Reynolds number > 10,000). The variable $\overrightarrow{F}_q$, on the other hand, represented both the centrifugal and the Coriolis forces that result from the use of the multiple reference frame (MRF) approach to capture the rotational motion of the stirrers. Finally, $\overrightarrow{R}_{pq}$ represented the interphase interaction forces between the continuous aqueous phase and the dispersed phase. Though different interphase interaction forces such as lift, virtual mass, wall lubrication, and drag forces are known to occur, only the drag force was accounted for as it has been shown to be the most significant interphase force in stirred tanks (Buffo et al., 2012; Khopkar et al., 2005; Maluta et al., 2021). Thus, the term $\overrightarrow{R}_{pq}$ was expanded as illustrated in equation (5) below.

$$\overrightarrow{R}_{pq} = -\overrightarrow{R}_{qp} = K_{pq}\left(\overrightarrow{V}_p - \overrightarrow{V}_q\right); \quad K_{pq} = \frac{3}{4}\alpha_q \alpha_p \rho_q \frac{C_D}{d_p}\left|\overrightarrow{V}_p - \overrightarrow{V}_q\right| \tag{5}$$

In this equation, $\overrightarrow{V}_p$ and $\overrightarrow{V}_q$ represented the phase velocities whereas K_{pq} represented the interphase exchange coefficient. In addition, d_p represented the diameter of the dispersed phase droplet whose value was approximated based on a well-developed correlation as shown in equation (6) (Peters, 1997). In this equation, the droplet diameter was related to the turbulence levels in the stirred tank through the Weber number (We) that is computed based on the the interfacial tension (σ_{pq} with value of 0.0511 N/m(Saien et al., 2014)), the impeller diameter (D) and the rotational speed (N), with values ranging from 46.97 to 237.81 depending on the rotational speed used. The effect of increasing the volume fraction of the dispersed phase on the droplet size was represented by the $(1 + \chi\alpha_{p,av})$ term in which $\alpha_{p,av}$ accounted for the average volume fraction of the dispersed solvent phase, while χ and A represented parameters that have been derived from several experimental studies (Cheng et al., 2017; Li et al., 2012). Average values of 5.01 and 0.054 (Cheng et al., 2017; Li et al., 2012) were respectively used in this study giving rise to droplets whose size was in the range of 182–482μ m.

$$\frac{d_p}{\mathrm{D}} = A(1 + \chi\alpha_{p,av})(We)^{-0.6}; We = \left(\frac{\rho_q N^2 D^3}{\sigma_{pq}}\right) \tag{6}$$

The term C_D in equation (5) represented the drag coefficient and this was specified based on the Schiller-Naumann model due to the small size of the droplets that implied rigid behaviour of the particles. The Schiller-Naumann model was represented in equation (7)–(8) where Re represented the droplet Reynolds number (ANSYS, 2018).

$$C_D = \begin{cases} \frac{24}{Re}\left(1 + 0.15Re^{0.687}\right) Re \le 1000 \\ 0.44 Re > 1000 \end{cases} \tag{7}$$

$$Re = \frac{\rho_q\left|\overrightarrow{V}_p - \overrightarrow{V}_q\right| d_p}{\mu_q} \tag{8}$$

As for turbulence modelling, a Reynolds-averaged approach was used to resolve turbulent fluctuations (see equations (3) and (4)). Furthermore, the Reynolds stresses arising from this approach were modelled based on Boussinesq's hypothesis that relates the fluctuating components to gradients of the mean velocity using the eddy viscosity (ANSYS, 2018). The latter, that is the eddy viscosity ($\mu_{t,m}$ in equation (4)), was expanded in terms of the turbulent kinetic energy (k) and the energy dissipation rate (ε) according to the mixture k-ε turbulence model. This is shown in equations 10–12. This turbulence modelling approach was chosen since it is appropriate for stratified multiphase flows (ANSYS, 2018) and this was an expected feature in the settler section of the SPB.

$$\mu_{t,m} = C_\mu \rho_m \frac{k^2}{\varepsilon} \tag{9}$$

$$\frac{\partial}{\partial t}(\rho_m k) + \nabla \cdot \left(\rho_m \overrightarrow{V_m} k\right) = \nabla \cdot \left(\left(\mu_m + \frac{\mu_{t,m}}{\sigma_k}\right)\nabla k\right) + G_{k,m} - \rho_m \varepsilon \tag{10}$$

$$\frac{\partial}{\partial t}(\rho_m \varepsilon) + \nabla \cdot \left(\rho_m \overrightarrow{V_m} \varepsilon\right) = \nabla \cdot \left(\left(\mu_m + \frac{\mu_{t,m}}{\sigma_\varepsilon}\right)\nabla \varepsilon\right) + \frac{\varepsilon}{k}\left(C_{1\varepsilon} G_{k,m} - C_{2\varepsilon}\rho_m \varepsilon\right) \tag{11}$$

In the equations above, C_μ, $C_{1\varepsilon}$, $C_{2\varepsilon}$, σ_k and σ_ε represented constants whose values are given in Table 2 below. Parameter $G_{k,m}$ represented the generation of turbulent kinetic energy from gradients of the mixture mean velocities (see equation (12)). Parameter ρ_m represented the mixture density (see equation (13)), μ_m represented the mixture viscosity (see equation (14)) and $\overrightarrow{V_m}$ represented the mixture velocity (see equation (15)).

$$G_{k,m} = \mu_{t,m}\left(\left(\nabla \overrightarrow{V_m}\right) + \left(\nabla \overrightarrow{V_m}\right)^T\right) : \nabla \overrightarrow{V_m} \tag{12}$$

$$\rho_m = \alpha_p \rho_p + \alpha_q \rho_q \tag{13}$$

Table 2
Mixture k-ε model constants.

C_μ	$C_{1\varepsilon}$	$C_{2\varepsilon}$	σ_k	σ_ε
0.09	1.44	1.92	1.00	1.30

$$\mu_m = \alpha_p \mu_p + \alpha_q \mu_q \tag{14}$$

$$\overrightarrow{V_m} = \frac{\alpha_p \rho_p \overrightarrow{V_p} + \alpha_q \rho_q \overrightarrow{V_q}}{\alpha_p \rho_p + \alpha_q \rho_q} \tag{15}$$

2.4.2. Model description (species transport)

Similar to the previous CFD study (Teke et al., 2022a), the production and extraction of lactic acid (a sample bioproduct that inhibits cell growth when the concentration is too high) in the SPB was studied so as to provide insight into the mass transfer behaviour of the system. A key difference between this work and the previous study (Teke et al., 2022a) was that the current work considered multiple phases (liquid–liquid SPB system) and was thus more realistic. The relevant governing equations describing the transport of lactic acid (species of interest) were as illustrated below.

$$\frac{\partial}{\partial t}(\alpha_q C_q) + \nabla \cdot \left(\alpha_q C_q \overrightarrow{V_q}\right) = -\nabla \cdot \left(\alpha_q \left(D_q + \frac{\mu_{t,m}}{\rho_q Sc_t}\right) \nabla C_q\right) + \alpha_q S_q - K_L a (m C_q - C_p) \tag{16}$$

$$\frac{\partial}{\partial t}(\alpha_p C_p) + \nabla \cdot \left(\alpha_p C_p \overrightarrow{V_p}\right) = -\nabla \cdot \left(\alpha_p \left(D_p + \frac{\mu_{t,m}}{\rho_p Sc_t}\right) \nabla C_p\right) + K_L a (m C_q - C_p) \tag{17}$$

In the above equations, C_i represented the concentration of lactic acid in phase i while D_i represented the molecular diffusion coefficient of the lactic acid in phase i. The molecular diffusion coefficients of lactic acid in the aqueous phase was set to 2.88×10^{-9} m^2/s (Bassi et al., 1987; Øyaas et al., 1995; Ribeiro et al., 2005; Siparsky et al., 1997; Wang et al., 2019) while the molecular diffusion coefficient of lactic acid in the organic solvent phases was set to 1.16×10^{-9} m^2/s (Wasewar et al., 2002). The latter value was an estimate based on the molecular diffusivity of lactic acid in methyl isobutyl ketone solvent. It should be noted that there is insufficient information on diffusivity of lactic acid in organic solvents in literature and this represents an area which needs further investigation.

A volumetric source term (S_q) of 6.20 g L^{-1} h^{-1}, based on literature (Chen and Ju, 2002; Oh et al., 2003; Yao and Toda, 2008), was introduced in the governing equation of the aqueous phase to represent the production of lactic acid by the cells in the mixer and settler sections of the SPB. It was assumed that no production would occur in the organic phase based on experimental observation that the cells chiefly resided in the aqueous phase. It should also be noted that the assumption of production within the settler was based on an expectation that there would be cells in the settler (although the majority would reside in the mixer). Because of these cells in the settler, some production would occur there, albeit at a limited extent, due to possible nutrient limitations and poor mass transfer in this section. As this has not been previously measured, a production value of 6.20 g L^{-1} h^{-1} (similar to that in mixer) was assumed as a first approximate.

Mass transfer of lactic acid across the aqueous phase-organic droplet interface was captured as a product of the overall mass transfer coefficient ($K_L a$) and the concentration driving force ($mC_q - C_p$). The former, that is the overall mass transfer coefficient, was modelled as a product of the mass transfer coefficient (K_L) and the interfacial area (a). The mass transfer coefficients in both the continuous aqueous phase (k_q) and the dispersed organic phase (k_p) were considered in generating the overall mass transfer coefficient as illustrated in equation (18) below. This expression was based on the Whiteman two-film theory, with m representing the distribution (partition) coefficient between the phases. The latter was initially set to 3.4 based on extractive fermentation values gotten from literature where n-hexane is used as an extractant and diluent during lactic acid removal (Matsumoto et al., 2003). However, experiments were done later and this value has been experimentally confirmed as 3.56 ± 0.05 (see Fig. 1 in the supplementary document).

$$\frac{1}{K_L} = \frac{m}{k_q} + \frac{1}{k_p} \tag{18}$$

In the choice of appropriate k_q and k_p correlations, it was necessary to take into account the size of the droplets as well as the turbulent conditions expected in the larger portion of the SPB. For the continuous phase side of the mass transfer interface, the model proposed by Batchelor (Batchelor, 1980; Jasińska et al., 2013) for small (rigid) spherical particles in turbulent conditions was chosen and this is given in equation (19) below. This equation accounts for mass transfer from the surface of a particle into a fluid due to molecular diffusion as well as convective motion.

$$k_q = 2\frac{\mathscr{D}_q}{d_p} + 0.689\left(\frac{\mathscr{D}_q{}^2}{d_p}\right)^{1/3}\left(\frac{\varepsilon}{\nu}\right)^{1/6} \tag{19}$$

For the dispersed phase or droplet side of the mass transfer interface, Young and Korchinsky (Young and Korchinsky, 1989) have proposed a model that addresses the impact of continuous phase turbulence on mixing within the dispersed phase droplet (see equation (20) below). Their approach uses an overall effective diffusivity expression that accounts for the mixing induced by turbulence. However, there is a need to experimentally determine the proportionality constant Λ, which is specific to the liquid–liquid system used (Young and Korchinsky, 1989). Given the lack of a general value of the constant, equation (21) was adopted where only mass transfer due to molecular diffusion is considered. This can be considered to be a limiting case of equation (20).

$$k_p = \frac{2\pi^2}{3d_p} \times \left(D_p + \frac{\Lambda \mathrm{x}\, 11 \mathrm{x} \rho_p \,\mathrm{x} d_p{}^{11/3} \mathrm{x} \varepsilon^{2/3}}{960 \sigma_{pq}}\right) \tag{20}$$

$$k_p = \frac{2\pi^2 D_p}{3d_p} \tag{21}$$

Finally, extraction of the lactic acid (species of interest) from the SPB was implemented based on liquid–liquid separation principles. The lactic acid, having been produced in the aqueous phase partitioned into the organic phase and this phase eventually settled as the top layer in the settler region of the SPB. The removal/extraction of a portion of this top layer (and hence a portion of the lactic acid) was implemented by specifying a velocity outlet term at the settler's top surface. To maintain a constant volume in the SPB, an equal amount of organic phase was re-introduced into the mixer section of the SPB by specifying a velocity inlet term on a portion of the mixer's top surface. In this case, the lactic acid concentration at the inlet was set to zero to represent "complete" back-extraction of lactic-acid from the recycled organic phase. In reality, however, a small concentration of the product could return in the recycled solvent/organic phase depending on the design of the back-

extraction unit. It should be noted that only a subset of the experimental volumetric extraction terms were tested for the CFD model (15 and 60 ml/min).

2.4.3. Computational procedure and validation

The governing fluid flow equations for the multiphase SPB system were solved using ANSYS Fluent 19.2 software, with the computational procedure adopted being largely similar to that used in the previous study (Teke et al., 2022a). Highlights of the procedure included the choice of meshing (hybrid mesh with primarily tetrahedral elements, ~766000 cells), resolution of impeller motion using the multiple reference frame (MRF) approach, the choice of boundary conditions (no-slip for walls with standard wall functions, slip for top surfaces), the choice of discretization schemes (first-order upwinding), the choice of timestep as the solution advances to steady-state (0.001 s) and the convergence criteria (residuals < 10^{-3}).

Once steady state was achieved for the governing flow equations, the species transport equations were turned on and these two sets of equations were solved simultaneously. The justification for this was illustrated in the previous study (Teke et al., 2022a) where it was shown that the flux (fluid exchange) between the mixer and the settler sections of the SPB was time-dependent and could not be accurately approximated based on frozen velocity fields. For this combined set of equations, a time step of 0.001 s was employed. The convergence residuals of 10^{-10} and 10^{-3} was set for the species transport and flow equations, respectively.

With regards to validation, it must be noted that an initial round of model validation was done and previously reported for the single-phase CFD model (Teke et al., 2022a). The said validation was done by comparing the model's prediction of flow parameters (power number, pumping number) as well as mass transfer parameters (mixing time) to experimental values. As the current study is an extension of the previously validated model to account for multiple phases, fewer validation experiments were done and these mainly focused on phase separation in the settler (with and without top-phase extraction) as described in section 2.3. Both qualitative and quantitative comparisons of the model's predictions and experimental observations have been done.

3. Results and discussion

This section presents investigations into the hydrodynamics and mass transfer of a multiphase SPB system. As a start, the validation of the multiphase model plus a discussion of the hydrodynamics involved is presented. Thereafter, the mass transfer behaviour of the system is presented and discussed. Insights into the operation of the multiphase SPB have been derived from these results and these will be useful for bioprocess engineers looking to operate *in situ* extractive fermentation systems, particularly in an SPB.

3.1. Model validation and hydrodynamics of the SPB

3.1.1. Phase separation without top-phase extraction

The CFD model was largely able to replicate the experimentally observed phase separation behaviour in the absence of top-phase extraction. Fig. 2 below shows that for the different agitation speeds tested, the CFD model predicted the amount of organic phase within the settler to within 10 % of the experimentally measured values. Fig. 3 and Fig. 4, on the other hand, give a qualitative comparison to accompany the results shown in Fig. 2. Here, it can be seen that the CFD model captured not only the phase separation in the settler section, but the mixing behaviour in the mixer section as well.

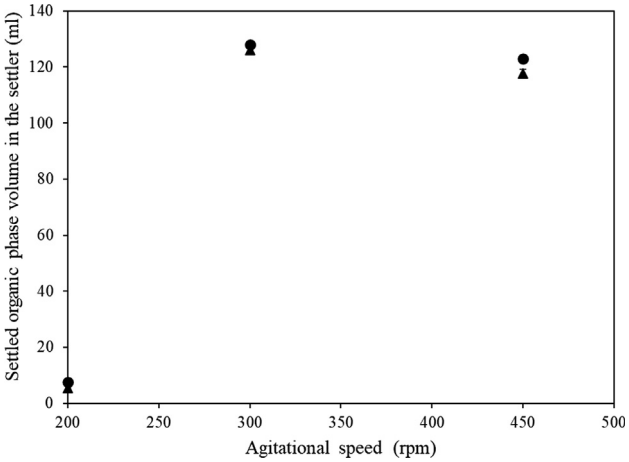

Fig. 2. Volume of settled organic phase (top phase) in the settler for various agitation speeds (rpm). The solid circles (●) represents CFD model results after steady state has been achieved (100 s for 200 rpm, 520 s for 300 rpm and 460 s for 450 rpm). The solid triangles (▲) represents experimental points with error bars included to illustrate the computed standard deviations from triplicate experimental runs.

From the contour maps and the experimental images, it can be seen that there was a poor drawdown of the buoyant organic phase at 200 rpm as evidenced by the concentration of the stained organic phase (red colour) near the top of the mixer section (see Fig. 4). Consequently, only a small amount of the organic phase was dispersed and made its way into the settler through the mixer-settler inter-compartmental opening per unit time. This led to small volumes of the organic phase in the settler in the short term (30 min as set in section 2.3.1) as illustrated in Fig. 2. It must be noted, however, that for the experimental runs conducted for longer durations (8 – 12 h), the volume of the organic phase is the settler at 200 rpm was observed to increase until values similar to those at other agitation rates were achieved. The fact that the drawdown and intercompartmental exchange of the organic phase occurred very slowly suggests that for practical design purposes, 200 rpm was not a suitable agitation rate (for this specific system). Note that for the SPB to operate well the extractant phase should be well and quickly dispersed (at whatever agitation rate is required to achieve that).

Increasing the agitation rate from 200 rpm resulted in better phase dispersion in the mixer as captured by both the CFD and experimental images (see Fig. 3 and Fig. 4). This led to increased draw-down of the organic phase and its dispersion, consequently leading to increased movement of the organic phase into the settler section per unit time (higher volumes in settler as indicated in Fig. 2). Between 300 rpm and 450 rpm, a slight decrease in the volume of the settled out organic phase (top phase) in the settler was noted. This was despite the expectation that increased agitation rates would lead to increased draw-down of the organic phase in the mixer, higher fluxes across the inter-compartmental opening and increased volumes of the organic phase in the settler. One phenomenon which might account for this is that increased flux magnitudes across the inter-compartmental opening led to an increase of the agitation level within the settler and thus the settling dynamics within the settler were disturbed close to the entry. Fig. 5 shows that as the agitation rate was increased, the velocity jet of the flux into the settler interacted with the back wall of the settler creating vortices within the settler. These vortices represent areas of increased mixing (hence interfering with the settling dynamics) and can be expected to increase with agitation rate.

As a final note on the hydrodynamics, it can be seen from Figs. 2 – 4 that the role of the agitation speed in the operation of an SPB

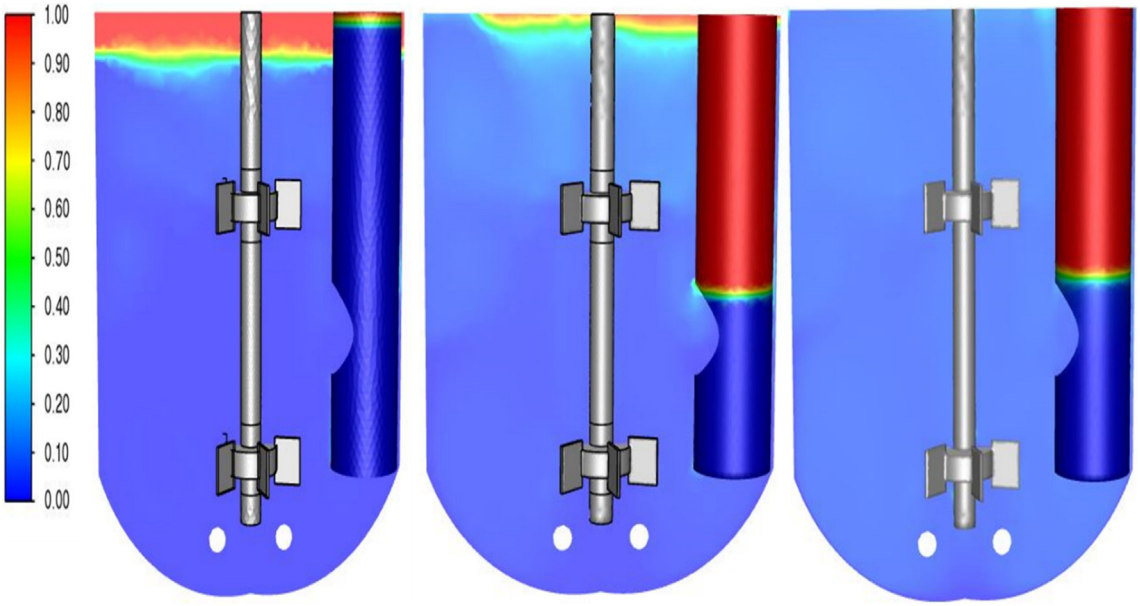

Fig. 3. Contour maps of the volume fraction of the organic phase showing the effect of agitation speed. Left side – 200 rpm, middle – 300 rpm and right side – 450 rpm.

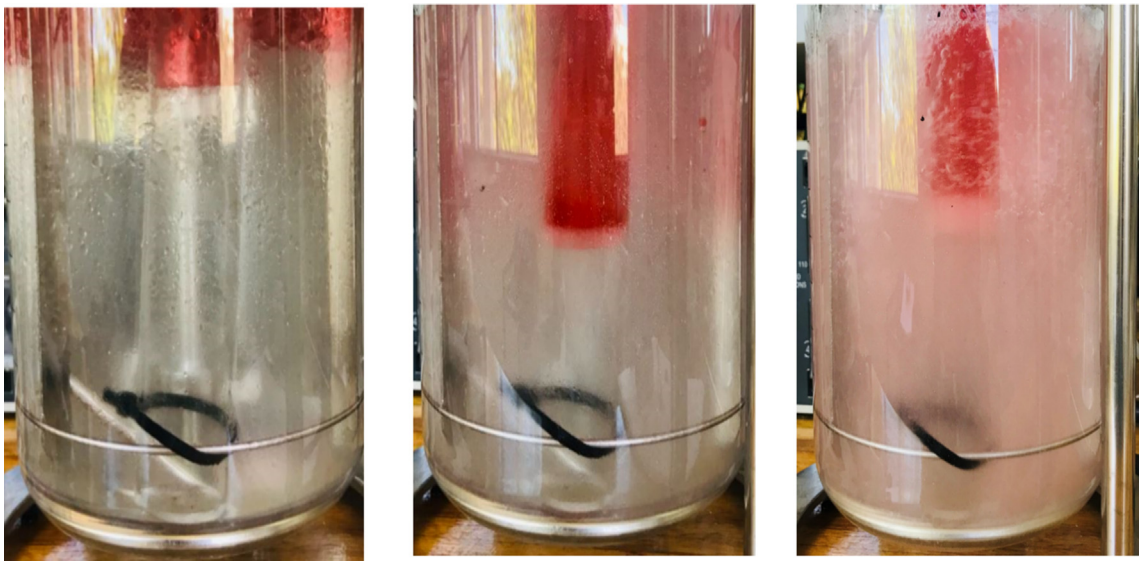

Fig. 4. Experimental pictures of the *n*-hexane/water system in the semi-partition bioreactor with the *n*-hexane stained with Red Oil O dye. Left side – 200 rpm, middle – 300 rpm and right side – 450 rpm.

cannot be understated. Keeping in mind that in the design of an SPB homogenous mixing needs to be achieved in the mixer section to allow for rapid product partitioning across the liquid–liquid phases (smaller droplets with high surface area, good dispersion increasing mass transfer), it can be seen that the agitation rate plays a role in achieving the desired degree of homogeneity. As shown in Fig. 3 and Fig. 4, the impellers were not able to fully drawdown and disperse the buoyant organic phase at 200 rpm. Thus, a large portion of the secondary organic phase remained/returned to the top of the mixer section. Increasing the agitation rate (from 300 to 450 rpm), however, resolved this issue. There was increased drawdown and dispersion of the organic phase within the mixer and this was accompanied with stronger inter-compartmental exchange/flux which resulted in more of the organic phase getting into the settler section. These results suggest that there will be a minimum agitation speed for each SPB design that will ensure the system's homogeneity in the mixer section. This minimum agitation speed is expected to be influenced by the geometry of the system and the liquid–liquid combination chosen. The latter is expected to be important since buoyancy depends on density differences. Hence, a designer must consider a sufficient (minimum) agitation speed that will allow for a good degree of dispersion within the mixer section. For this study, sufficient dispersion was achieved at an agitation rate of 300 rpm and this value was adopted for further experiments.

It should also be noted that in selecting a minimum agitation speed that gives sufficient dispersion (e.g. 300 rpm, as chosen above), a bioreactor designer would want to consider the magnitude of shear stress that the micro-organisms can tolerate since the latter prefer low-shear environments. In a stirred tank system, the impeller motion is responsible for the generation of velocities and hence high shear rates are found near the impellers. Fig. 6

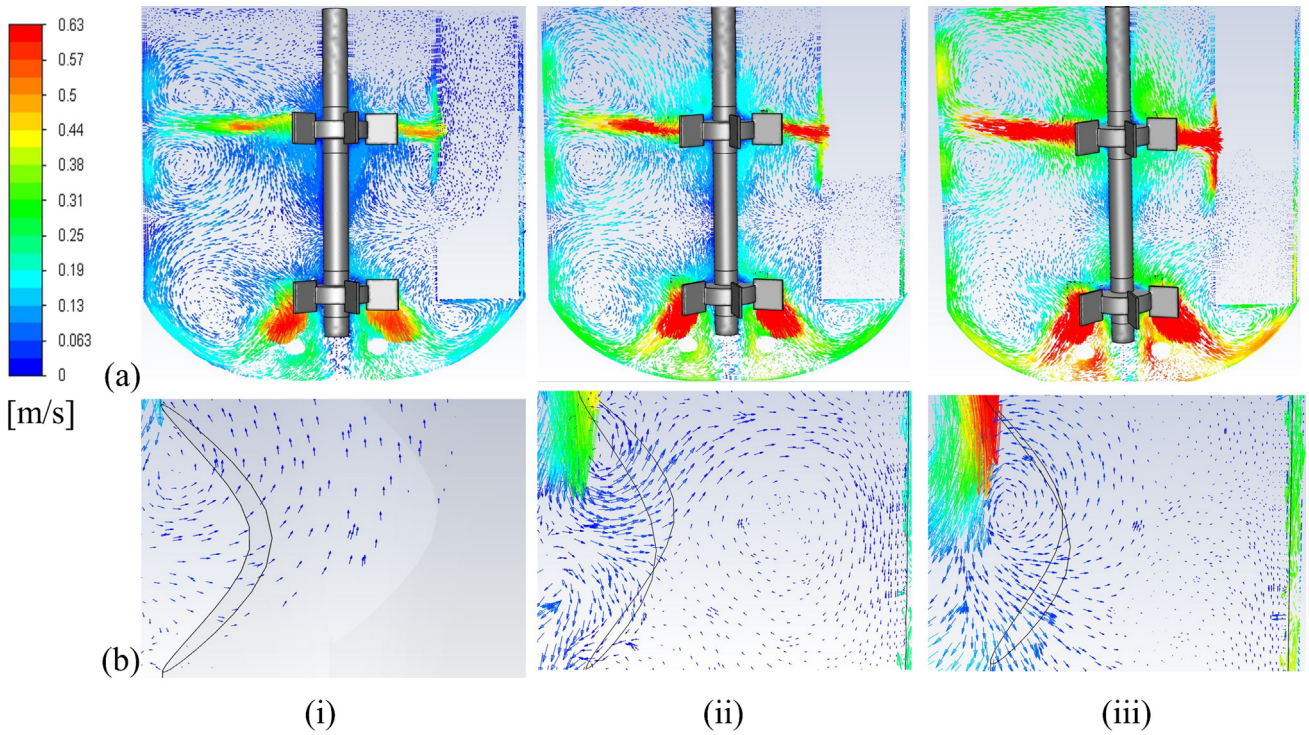

Fig. 5. Instantaneous velocity vectors after steady state is achieved in the CFD simulations (different times required for each simulation) showing the degree of interaction between the mixer and settler sections. Simulation at different agitation rates – (i) 200 rpm, (ii) 300 rpm, and (iii) 450 rpm. Top row (a) – view of the entire SPB plotted on a plane that cuts across the inter-compartmental opening. Bottom row (b) – an expanded view of the inter-compartmental opening.

below shows a contour map of the CFD-predicted shear stresses in the SPB for agitation speeds of 200 – 450 rpm (computed as the product of viscosity (molecular and turbulent) and strain rate in Ansys Fluent). From this figure, it can be seen that increasing the agitation speed increases shear stresses with this being more evident around the impeller regions compared to the rest of the tank (see also Table 3 below).

The threshold for cell damage varies with cell type (bacteria, fungi, animal and algae (Arnaud et al., 1993; Bronnenmeier and Märkl, 1982; Edwards et al., 1989; Funahashi et al., 1987; Huang et al., 2016; Michels et al., 2010). Table 4 below shows an example of different cell types and their shear stress limits before cell damage. From this table and Table 3 above, it can be seen that the volume-averaged shear stresses are well within the tolerable shear limits of the given cells. However, the maximum shear stresses (near the impeller) are higher as compared to the volume average. An expectation will be that the shear stress dependency will rely on the micro-organism used, as different cell types will have different limits for their viability (see Table 4 below). This can be indirectly affirmed by the fact that the authors have successfully grown *Lactobacillus* sp. at the chosen agitation speed (300 rpm) in this reactor (Teke et al., 2022b).

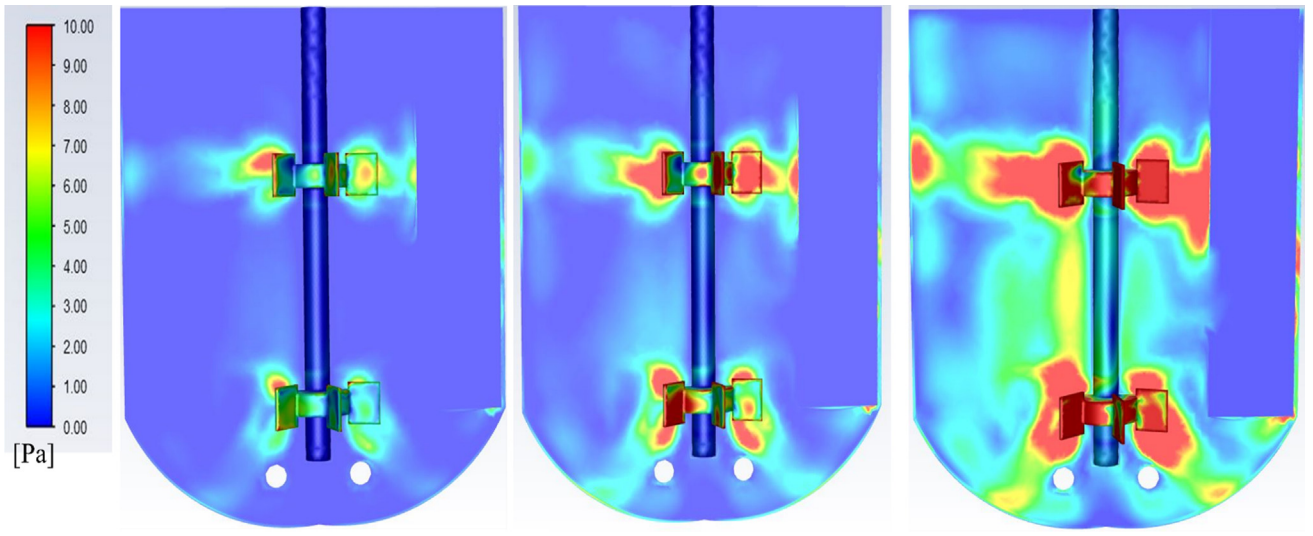

Fig. 6. Shear stress contour maps of a plane in the SPB showing the effect of agitation speed. Left side – 200 rpm, middle – 300 rpm and right side – 450 rpm.

Table 3
CFD-predicted shear stresses based on the changes in agitation speed in the SPB.

Agitation Speed (rpm)	Volume-averaged shear stress (Pa)	
	Impeller regions	Rest of tank excluding impellers
200	2.64	0.50
300	5.36	1.06
450	13.35	2.59
	Maximum shear stress (Pa)	
200	59.03	14.81
300	152.70	28.61
450	304.34	52.17

Table 4
Shear stress limits for different micro-organisms in literature.

Cell Type	Shear stress (Pa)	References.
Algae	0–500	(García Camacho et al., 2007; Huang et al., 2016; Michels et al., 2010; Scarsella et al., 2012)
Animal	0.2–150	(Chittur et al., 1988; Godoy-Silva et al., 2009; Odeleye et al., 2014; Petersen et al., 1988)
Fungi	0–40	(Edwards et al., 1989; Mitard and Riba, 1988)
Bacteria	0–2770	(Arnaud et al., 1993; Funahashi et al., 1987; García et al., 2019; Lange et al., 2001)

3.1.2. Phase separation with top-phase extraction

Fig. 7 below depicts the results of the phase separation experiments with continuous volumetric removal of the top (settled out) phase from the settler section. Only the results for 300 rpm are shown as this agitation rate was chosen for all further experiments based on observations of phase dispersion or system homogeneity within the mixer (see section 3.1.1). It can be seen that the CFD model was able to correctly predict the amount of organic phase that would be left in the settler section as the top phase, with CFD predictions accurate to within 12 % in comparison with the experimental values. Note that the amount of the organic phase remaining in the settler was a function of (i) the mixing dynamics in the mixer section (draw-down of buoyant organic phase and subsequent phase dispersion), (ii) the flux across the inter-compartmental opening, (iii) the settling dynamics or phase separation in quiescent settler section due to density differences (buoyancy force) and (iv) the volumetric extraction rate. Fig. 7 illustrates that for a given set of conditions (i) – (iii), the rate of volumetric extraction determines the amount of the top phase (settled out organic phase) remaining in the settler section. Alternatively stated, for a given set of conditions (i) – (iii), setting the amount of the top phase in the settler section (can also be referred to as a buffer) as the design objective sets the maximum possible volumetric extraction rate. Examining Fig. 7 from the perspective of setting the buffer volume as a design objective may be important when one considers that the undesirable situation where the volumetric extraction rate can be set to too a high value such that the primary liquid phase ends up being removed – i.e., when the fermentation media is withdrawn from the bioreactor and directed to the back extraction unit. It should, however, be noted that this maximum possible volumetric extraction rate only serves as an upper limit. A more optimal value may be obtained by setting a different design objective that includes cell activity (production). The latter is not accounted for in the phase separation results discussed so far in this section.

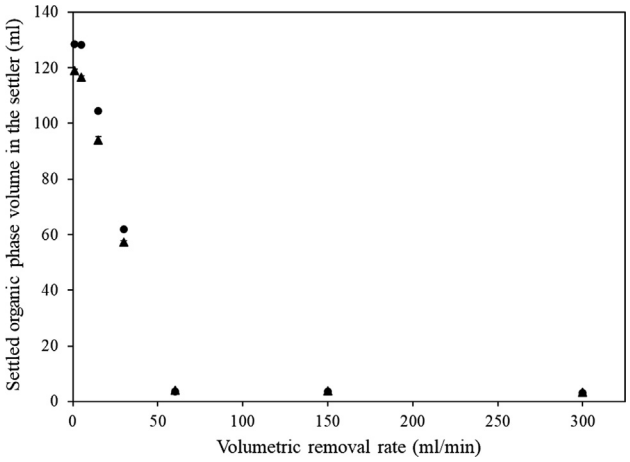

Fig. 7. Volume of the top (settled out) organic phase in settler versus volumetric removal rate at 300 rpm for both experiments and CFD simulations. The solid symbols (●) represents CFD modelling results and the symbol (▲) represents experimental points with error bars included to indicate the standard deviations from triplicate experimental runs.

3.2. Species transport within the liquid–liquid SPB

3.2.1. Species transport within the mixer section

The results from the CFD runs involving production and extraction of lactic acid (at different volumetric removal rates) are shown in Fig. 8. It must be noted that these simulations were run for a shorter duration (less than 7 min of simulation time) in comparison to the previous single-phase CFD study where simulations were conducted for 70 – 90 min of simulation time (Teke et al., 2022a). For the multiphase CFD model, the need to run both the species equations plus the multiphase flow equations simultaneously to capture the transient inter-compartmental flux behaviour resulted in a higher computational requirement (and hence higher physical time requirement). This presents a shortcoming in the use of the current CFD model to investigate species transport in the multiphase SPB which may be addressed by the use of synergistic models that have been proposed as a means to incorporate time-scales of both product formation and a reactor's hydrodynamics (Anye Cho et al., 2021).

Despite the above shortcoming, some insights can be gained from the results in Fig. 8. It can be seen, for example, that an increase in the volumetric removal rate reduced the concentration of the product accumulated in the mixer section. This drop was noted for both the aqueous phase and the organic phase. Two reasons may be suggested for the noted drop; first, the effectiveness of liquid–liquid partitioning of the product (mass transfer) followed by flux of the liquid–liquid mixture into the settler, phase separation in the settler and volumetric extraction of the product-rich top phase in the settler. The second reason may be the dilution of the product's concentration due to continuous inflow of the recycled and back-extracted organic phase with low (or zero) product concentration into the mixer (this inflow balances the volume being continuously extracted).

To assess which of these reasons suggested above is more likely, a comparison between the characteristic times involved in each may be done. Considering the replenishment of the organic phase by the recycled batch, one may consider an initial organic phase volume of 500 ml (10 % by volume *n*-hexane) and an extraction rate of 60 ml/min. For such conditions, the characteristic time for replenishment of the entire/initial organic phase would be 500 s ($500\ \text{ml} \times (60\ \text{ml/min})^{-1}$). On the other hand, for effective liquid–liquid partitioning (mass transfer) followed by flux of the liquid–liquid mixture into the settler, phase separation in the settler and volumetric extraction, one may consider the characteristic time to be a sum of the time for mass transfer, the time for flux across the inter-compartmental opening (inter-compartmental mixing), the time for phase separation and the time for volumetric extraction in the settler. The characteristic time of mass transfer in

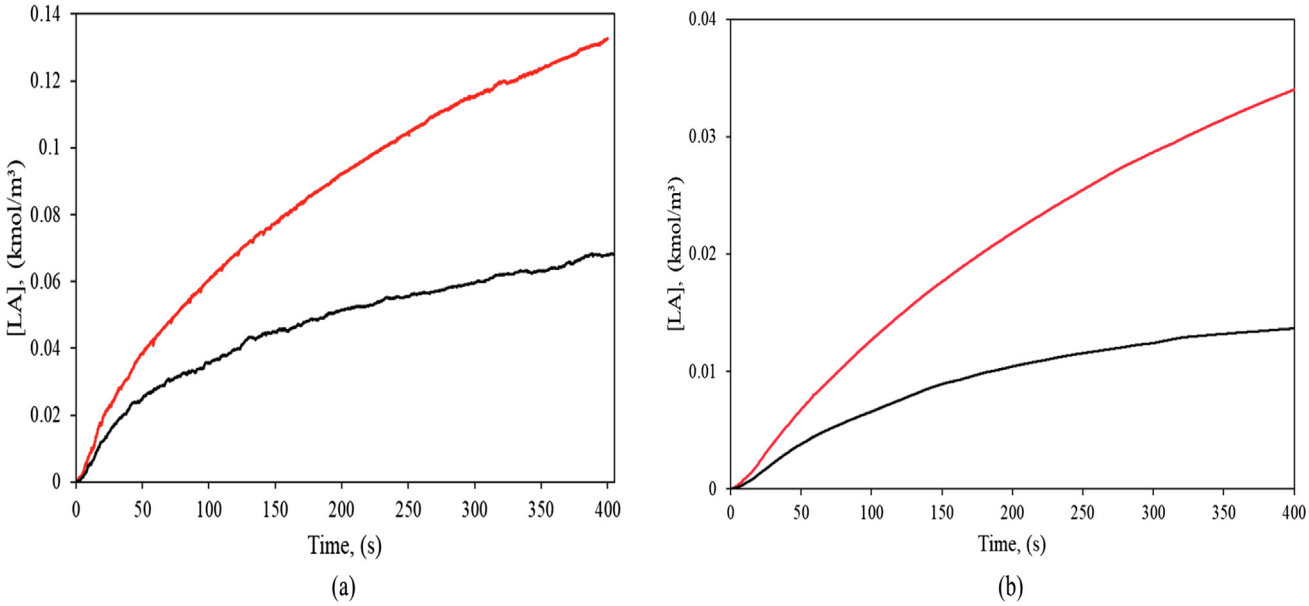

Fig. 8. Volume-averaged molar concentration of lactic acid versus time in the mixer based on CFD simulations. (a) Concentration of lactic acid in the aqueous phase, (b) Concentration of lactic acid in the organic phase. The solid red line (—) represents 15 ml/min removal rate. The black line (—) represents 60 ml/min removal rate.

the tank (mixer), computed as the inverse of the volume-averaged volumetric mass transfer coefficient (K_La), is approximately 52 s from the simulations (K_La calculated using custom function fields in ANSYS Fluent based on equations (18) – (21)). The time for inter-compartmental mixing can be assumed to be small due to generally rapid mixing at 300 rpm while the time for phase separation in the settler cannot be immediately established. However, the time of volumetric extraction can be estimated based on initial organic phase volume in settler (assuming no extraction) and the extraction rate. At 300 rpm, the initial organic phase volume in the settler (assuming no extraction) would be 128 ml as seen in Fig. 7. For a removal rate of 60 ml/min, the time for extraction would thus be 128 s (128 ml × (60 ml/min)$^{-1}$). Since phase separation in the settler has to be faster than the volumetric removal rate (from the settler) to ensure a buffer layer (top phase) is maintained (see Fig. 7), the time for phase separation will be less than or equal to 128 s. Thus, a total characteristic time may be estimated as about 308 s (52 + 128 + 128). This value is less than that obtained for the characteristic time for replenishment of the organic phase (500 s). Thus, it may be concluded that the reduction in lactic acid concentration upon increase in volumetric removal rate (as noted in Fig. 8) is more likely due to effective liquid–liquid partitioning (mass transfer) followed by the subsequent steps leading to volumetric extraction of the product-rich top phase in the settler.

An interesting question arising from the results in Fig. 8 touches on the observation that the concentration of the product in the aqueous phase remains higher than that in the organic phase although the organic phase has a higher absorption capacity for the lactic acid. This observation may be better seen in Fig. 9 where the ratio of lactic acid concentration in organic phase to lactic acid concentration in aqueous phase is less than unity (for the simulated time) though the experimental (or long term) partition coefficient was found to be 3.56 (see supplementary sheet). Though the current observation is based on short term simulations, one may ask whether this trend is maintained even in the long term due to the continuous extraction and replenishment of the organic phase in the SPB (note Fig. 9 shows that the ratio of concentrations is lower for higher extraction rates). If that is the case, it may then be suggested that one does not necessarily need a liquid–liquid system with a high partition coefficient since the full absorptive

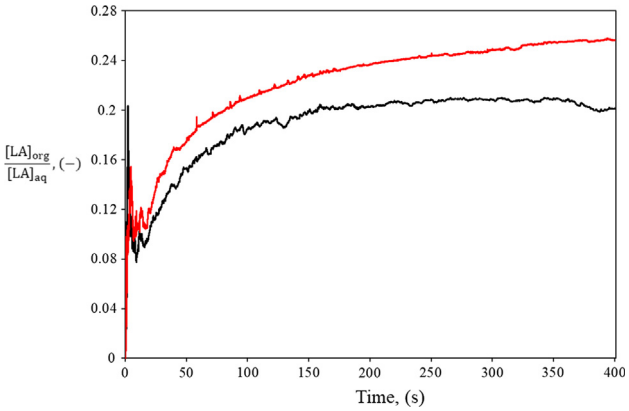

Fig. 9. Ratio of lactic acid concentration in organic phase to lactic acid concentration in aqueous phase plotted against time (mixer section considered). The experimental partition coefficient value is 3.4. The solid red line (—) represents 15 ml/min removal rate. The black line (—) represents 60 ml/min removal rate.

capacity of the organic phase is not actually utilized in the SPB design. Instead, cheaper combinations of liquid–liquid systems may be exploited with the decrease in concentration driving force (due to lower partition coefficient) being offset with an increase in the overall volumetric mass transfer coefficient (easily adjustable through agitation rate).

As noted earlier, the simulations were run for a short duration (less than 7 min of simulation time). In the previous single-phase study (Teke et al., 2022a), longer time durations were required to achieve equilibrium conditions in the concentration of the product. Thus, the equilibrium concentrations cannot be predicted or assessed based on these current results. In particular, the question as to whether the product inhibition limit (0.15 kmol m^{-3} for lactic acid) will be reached (or not) depending on the volumetric extraction rate cannot be currently answered. Though it is possible to predict this based on the current CFD model, the requirement for significantly longer run times was seen as a disadvantage by the authors who chose to rather run an actual growth experiment. The results of the growth experiment have been communicated

elsewhere (Teke et al., 2022b), but validate the work presented here.

3.2.2. Species transport within the settler section

From Fig. 10, it can be seen that an initial steep increase occurs in product concentration in the aqueous phase (within first 50 *sec*). The steep increase is probably due to the set-up of the CFD model and in particular the specification of a 6.20 g/L h productivity value in the settler (aqueous phase). Further evidence supporting this can be seen from time lag experienced before product concentration in the organic phase (in the settler) begins to rise (Fig. 10 (A)). This time lag is likely an indication of the mass transfer/liquid–liquid partitioning process within the settler. After the first 50 s, the product concentration in the aqueous phase begins to drop. This is likely due to the effectiveness of liquid–liquid partitioning to organic phase and organic phase (or top phase) extraction that is happening concurrently. It can be seen that low concentrations of the product (0.041 kmol m^{-3}) in the aqueous phase are maintained after about 150 s indicating that the influence of the productivity term specified in the settler is moderated in the long term.

As for the behaviour of lactic acid concentration in the organic phase, it can be seen that the concentration initially increases and peaks at about 100 s. This, as explained above, is likely due to mass transfer of lactic acid from the aqueous phase within the settler where a non-zero productivity term was set. The decrease in lactic acid concentration in the organic phase after 100 s is likely due to the effectiveness of top phase extraction. However, the concentration does not drop down to low levels as seen in the aqueous phase graph. This can be explained by recalling that the settler continually receives product-rich organic phase from the mixer as part of the liquid–liquid extractive fermentation process. This can be seen from the organic phase absorbed product concentrations of 0.012 and 0.013 kmol m^{-3} in the settler and mixer respectively after 400 s.

3.3. Expected changes in the presence of cells

In an actual extractive fermentation process, the growth of micro-organisms (biomass) will add to the complexity of the bioreactor design. It is important to anticipate and include possible changes that may be introduced by the micro-organisms into any CFD model developed for the process. The micro-organisms can be expected to have an effect on the droplet diameters of the secondary liquid phase (through surface tension), the viscosity and the mass transfer, just to mention a few parameters. For example, the measurement of the viscosity of an aqueous phase-biomass mixture illustrates that the growth of lactic acid bacteria (*Lactobacillus casei*) leads to an increase in viscosity. Fig. 11 illustrates this point with results provided at two temperatures – a lower temperature (25 °C) corresponding to the current model's physical properties and a higher temperature (37 °C) corresponding to the optimum production temperature for lactic acid bacteria. Since the viscosity does affect the hydrodynamics of a system, changes may be expected in the results reported so far. This simple example highlights the need for further work on the CFD model developed so far to incorporate changes introduced by the cells.

4. Conclusions

In this study, a two-fluid multiphase CFD model of the semi-partition bioreactor has been built. The model has been validated based on phase separation experiments and has been used to investigate the hydrodynamics and mass transfer in the multiphase SPB system. A summary of the key insights generated are presented below:

A minimum agitation rate for system homogeneity required – it has been observed that the agitation speed is a strong determinant of the system's homogeneity or phase dispersion in the mixer section. A minimum value of the agitation speed exists that allows for full dispersion of the organic phase in the mixer and a good inter-compartmental flux between the mixer and settler section. Any value below this agitation speed results in poor phase dispersion in the mixer. Thus, a designer should consider investigating this aspect to find the appropriate value for their system.

Mass transfer rate or extraction/replenishment rate as determining rate? A comparison between the characteristic time for mass transfer (liquid–liquid partitioning) and the characteristic time for replenishment of the organic phase (being continuously extracted) determines whether the reduction in concentration of the product

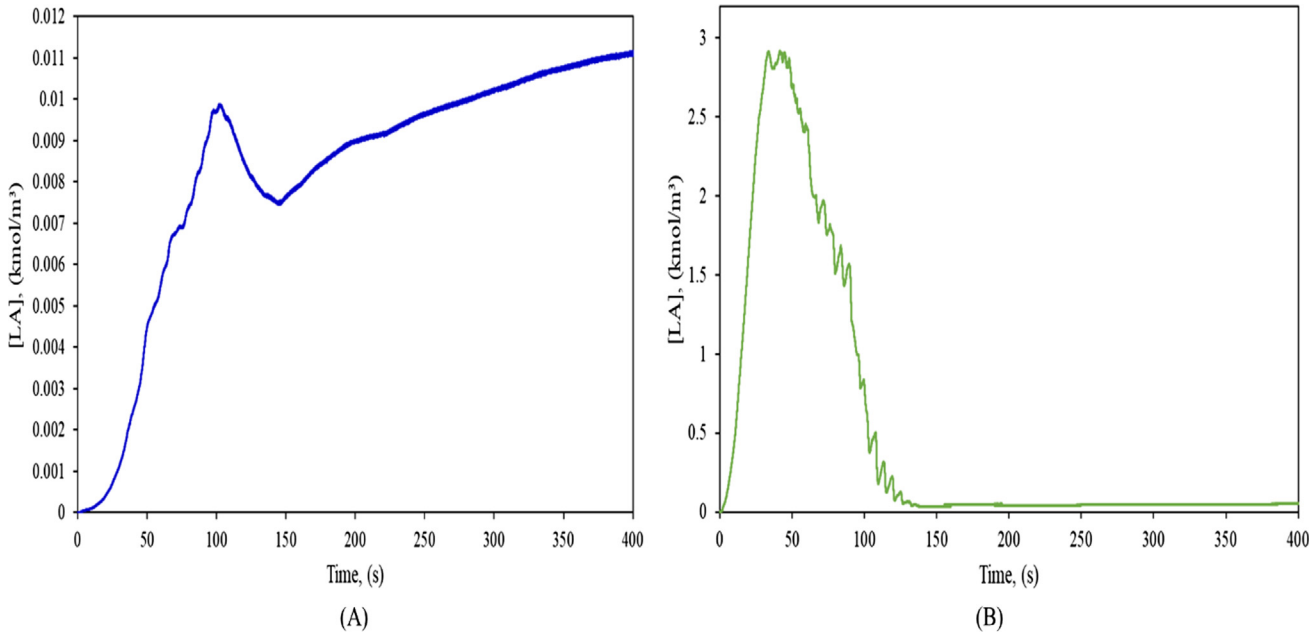

Fig. 10. Volume-averaged molar concentration of lactic acid versus time in the settler based on CFD simulations at 60 ml/min volumetric removal rate. (a) Concentration of lactic acid in the organic phase, (b) concentration of lactic acid in the aqueous phase.

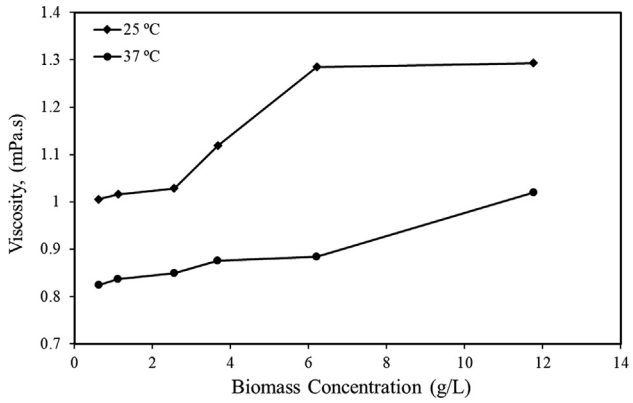

Fig. 11. Viscosity of aqueous phase-biomass mixture versus biomass growth concentration of lactic acid bacteria (Lactobacillus casei) at 25 °C and 37 °C.

of interest in the SPB is due to effective *in-situ* extraction or due to product dilution by the recycled and back-extracted batch of the organic phase. For the system considered, it was observed that effective liquid–liquid partitioning and subsequent steps leading to volumetric extraction was the determining rate. However, this conclusion is system-specific and should be investigated for different liquid–liquid combinations and different bio-products.

Necessity of a liquid–liquid system with a high partition coefficient – the results obtained illustrate that the absorptive capacity of the organic phase is not fully utilized (in the short term). If such a trend is maintained in the long term due to continuous extraction and replenishment of the organic phase, a design engineer can get away with using a liquid–liquid system with a lower partition coefficient value.

CRediT authorship contribution statement

George M. Teke: Conceptualization, Methodology, Software, Validation, Formal analysis, Investigation, Data curation, Writing – original draft, Visualization. **Godfrey K. Gakingo:** Conceptualization, Methodology, Software, Resources, Writing – review & editing, Supervision, Project administration. **Robert W.M. Pott:** Conceptualization, Methodology, Resources, Writing – review & editing, Supervision, Project administration, Funding acquisition.

Data availability

Data will be made available on request.

Declaration of Competing Interest

The authors declare that they have no known competing financial interests or personal relationships that could have appeared to influence the work reported in this paper.

Acknowledgements

G.M. Teke was fully funded research scholar under the Harry Crossley Foundation, South Africa. Also, this work was generously funded by Hortgro and the Postharvest Innovation Programme, South Africa. Finally, special thanks to the administrators at the Higher Performance Computing at Stellenbosch University and the Centre for High Performance Computing at Rosebank, Cape Town for their support.

Appendix A. Supplementary material

Supplementary data to this article can be found online at https://doi.org/10.1016/j.ces.2022.118226.

References

ANSYS, 2018. ANSYS Fluent Theory Guide-Release 19.2. *Basic fluid flow*.
Anye Cho, B., de Carvalho Servia, M.Á., del Río Chanona, E.A., Smith, R., Zhang, D., 2021. Synergising biomass growth kinetics and transport mechanisms to simulate light/dark cycle effects on photo-production systems. Biotechnol. Bioeng. 118, 1932–1942.
Arnaud, J.P., Lacroix, C., Foussereau, C., Choplin, L., 1993. Shear stress effects on growth and activity of Lactobacillus delbrueckii subsp. bulgaricus. J. Biotechnol. 29, 157–175 https://linkinghub.elsevier.com/retrieve/pii/016816569390048R.
Bassi, A.S., Rohani, S., Macdonaid, D.G., 1987. Measurement of Effective Diffusivities of Lactose and Lactic Acid in 3% Agarose Gel Membrane. Biotechnol. Bioeng. 30, 794–797.
Batchelor, G.K., 1980. Mass transfer from small particles suspended in turbulent fluid. J. Fluid Mech. 98, 609–623.
Bronnenmeier, R., Märkl, H., 1982. Hydrodynamic stress capacity of microorganisms. Biotechnol. Bioeng. 24, 553–578.
Buffo, A., Vanni, M., Marchisio, D.L., 2012. Multidimensional population balance model for the simulation of turbulent gas-liquid systems in stirred tank reactors. Chem. Eng. Sci. 70, 31–44. https://doi.org/10.1016/j.ces.2011.04.042.
Chen, C.C., Ju, L.K., 2002. Coupled lactic acid fermentation and adsorption. Appl. Microbiol. Biotechnol. 59, 170–174.
Cheng, D., Feng, X., Cheng, J., Yang, C., 2013. Numerical simulation of macro-mixing in liquid-liquid stirred tanks. Chem. Eng. Sci. 101, 272–282. https://doi.org/10.1016/j.ces.2013.06.026.
Cheng, D., Wang, S., Yang, C., Mao, Z.S., 2017. Numerical Simulation of Turbulent Flow and Mixing in Gas-Liquid-Liquid Stirred Tanks. Ind. Eng. Chem. Res. 56, 13050–13063.
Chittur, K.K., Mcintire, L.V., Rich, R.R., 1988. Shear Stress Effects on Human T Cell Function. Biotechnol. Prog. 4, 89–96.
Edwards, N., Beeton, S., Bull, A.T., Merchuk, J.C., 1989. A novel device for the assessment of shear effects on suspended microbial cultures. Appl. Microbiol. Biotechnol. 30, 190–195.
Funahashi, H., Maehara, M., Taguchi, H., Yoshida, T., 1987. Effects of agitation by flat-bladed turbine impeller on microbial production of xanthan gum. J. Chem. Eng. Japan 20, 16–22.
García, C., Bautista, L., Rendueles, M., Díaz, M., 2019. A new synbiotic dairy food containing lactobionic acid and Lactobacillus casei. Int. J. Dairy Technol. 72, 47–56.
García Camacho, F., Gallardo Rodríguez, J.J., Sánchez Mirón, A., Cerón García, M.C., Belarbi, E.H., Molina, G.E., 2007. Determination of shear stress thresholds in toxic dinoflagellates cultured in shaken flasks. Implications in bioprocess engineering. *Process Biochem.* 42, 1506–1515.
Godoy-Silva, R., Chalmers, J.J., Casnocha, S.A., Bass, L.A., Ma, N., 2009. Physiological responses of CHO cells to repetitive hydrodynamic stress. Biotechnol. Bioeng. 103, 1103–1117.
Huang, J., Ying, J., Fan, F., Yang, Q., Wang, J., Li, Y., 2016. Development of a novel multi-column airlift photobioreactor with easy scalability by means of computational fluid dynamics simulations and experiments. Bioresour. Technol. 222, 399–407. https://doi.org/10.1016/j.biortech.2016.09.109.
James, G., Görgens, J.F., Pott, R.W.M., 2021. Co-production of volatile fatty acids and biogas from an anaerobic digestion system using in situ extraction. Sep. Purif. Technol. 257, 117891.
Jasińska, M., Bałdyga, J., Cooke, M., Kowalski, A., 2013. Investigations of mass transfer with chemical reactions in two-phase liquid-liquid systems. Chem. Eng. Res. Des. 91, 2169–2178.
Khopkar, A.R., Rammohan, A.R., Ranade, V.V., Dudukovic, M.P., 2005. Gas-liquid flow generated by a Rushton turbine in stirred vessel: CARPT/CT measurements and CFD simulations. Chem. Eng. Sci. 60, 2215–2229.
Kuila, A., Sharma, V., 2018. Principles and Applications of Fermentation Technology. In: Arindam Kuila, Vinay Sharma (Eds.), first ed. John Wiley & Sons, Inc., Hoboken, NJ, USA, pp. 1–12. http://doi.wiley.com/10.1002/9781119460381.
Lange, H., Taillandier, P., Riba, J.P., 2001. Effect of high shear stress on microbial viability. J. Chem. Technol. Biotechnol. 76, 501–505.
Laurenzi, F., Coroneo, M., Montante, G., Paglianti, A., Magelli, F., 2009. Experimental and computational analysis of immiscible liquid-liquid dispersions in stirred vessels. Chem. Eng. Res. Des. 87, 507–514.
Li, S., Duan, W., Chen, J., Wang, J., 2012. CFD simulation of gas-liquid-liquid three-phase flow in an annular centrifugal contactor. Ind. Eng. Chem. Res. 51, 11245–11253.
Maluta, F., Paglianti, A., Montante, G., 2021. Two-fluids RANS predictions of gas cavities, power consumption, mixing time and oxygen transfer rate in an aerated fermenter scale-down stirred with multiple impellers. Biochem. Eng. J. 166,. https://doi.org/10.1016/j.bej.2020.107867 107867.
Matsumoto, M., Takahashi, T., Fukushima, K., 2003. Synergistic extraction of lactic acid with alkylamine and tri-n-butylphosphate: Effects of amines, diluents and temperature. Sep. Purif. Technol. 33, 89–93.

Michailidou, E.K., Assael, M.J., Huber, M.L., Perkins, R.A., 2013. Reference Correlation of the Viscosity of n-Hexane from the Triple Point to 600 K and up to 100 MPa. J. Phys. Chem. Ref. Data 42.

Michels, M.H.A., Van Der Goot, A.J., Norsker, N.H., Wijffels, R.H., 2010. Effects of shear stress on the microalgae Chaetoceros muelleri. Bioprocess Biosyst. Eng. 33, 921–927.

Mitard, A., Riba, J.P., 1988. Morphology and growth ofAspergillus niger ATCC 26036 cultivated at several shear rates. Biotechnol. Bioeng. 32, 835–840 https://onlinelibrary.wiley.com/doi/10.1002/bit.260320617.

Odeleye, A.O.O., Marsh, D.T.J., Osborne, M.D., Lye, G.J., Micheletti, M., 2014. On the fluid dynamics of a laboratory scale single-use stirred bioreactor. Chem. Eng. Sci. 111, 299–312. https://doi.org/10.1016/j.ces.2014.02.032.

Oh, H., Wee, Y.J., Yun, J.S., Ryu, H.W., 2003. Lactic acid production through cell-recycle repeated-batch bioreactor. Appl. Biochem. Biotechnol. - Part A Enzym Eng. Biotechnol. 107, 603–614.

Øyaas, J., Storrø, I., Svendsen, H., Levine, D.W., 1995. The effective diffusion coefficient and the distribution constant for small molecules in calcium-alginate gel beads. Biotechnol. Bioeng. 47, 492–500.

Peters, D.C., 1997. Dynamics of emulsification. In: Harnby, A.W., Edwards, N., Nienow, M.F. (Eds.), *Mix. Process Ind.* Butterworth−Heinemann, Oxford, UK, pp. 294–324.

Petersen, J.F., McIntire, L.V., Papoutsakis, E.T., 1988. Shear sensitivity of cultured hybridoma cells (CRL-8018) depends on mode of growth, culture age and metabolite concentration. J. Biotechnol. 7, 229–246.

Ribeiro, A.C.F., Lobo, V.M.M., Leaist, D.G., Natividade, J.J.S., Veríssimo, L.P., Barros, M. C.F., Cabral, A.M.T.D.P.V., 2005. Binary diffusion coefficients for aqueous solutions of lactic acid. J. Solution Chem. 34, 1009–1016.

Saien, J., Rezvani Pour, A., Asadabadi, S., 2014. Interfacial tension of the n-hexane-water system under the influence of magnetite nanoparticles and sodium dodecyl sulfate assembly at different temperatures. J. Chem. Eng. Data 59, 1835–1842.

Scarsella, M., Torzillo, G., Cicci, A., Belotti, G., De Filippis, P., Bravi, M., 2012. Mechanical stress tolerance of two microalgae. Process Biochem. 47, 1603–1611. https://doi.org/10.1016/j.procbio.2011.07.002.

Siparsky, G.L., Voorhees, K.J., Dorgan, J.R., Schilling, K., 1997. Water transport in polylactic acid (PLA), PLA/polycaprolactone copolymers, and PLA/polyethylene glycol blends. J. Environ. Polym. Degrad. 5, 125–136.

Stanbury, P.F., Whitaker, A., Hall, S.J., 2017. Principles of Fermentation Technology. In: Fiona Geraghty (ed.), third ed., Elsevier, pp. 1–19. https://linkinghub.elsevier.com/retrieve/pii/C20130001867.

Stark, D., von Stockar, U., 2003. In Situ Product Removal (ISPR) in Whole Cell Biotechnology During the Last Twenty Years. In: *Process Integr. Biochem. Eng.*, vol. 80, pp. 149–175. http://link.springer.com/10.1007/3-540-36782-9_5.

Teke, G.M., Pott, R.W.M., 2021. Design and evaluation of a continuous semipartition bioreactor for in situ liquid-liquid extractive fermentation. Biotechnol. Bioeng. 118, 58–71 https://onlinelibrary.wiley.com/doi/10.1002/bit.27550.

Teke, G.M., Tai, S.L., Pott, R.W.M., 2021. Extractive Fermentation Processes: Modes of Operation and Application. ChemBioEng Rev. 9, 1–19 https://onlinelibrary.wiley.com/doi/10.1002/cben.202100028.

Teke, G.M., Gakingo, G.K., Pott, R.W.M., 2022a. Towards improved understanding of the hydrodynamics of a semi-partition bioreactor (SPB): a numerical investigation. Chem. Eng. Res. Des. 177, 210–222. https://doi.org/10.1016/j.cherd.2021.10.026.

Teke, G.M., Gakingo, G.K., Pott, R.W.M., 2022b. The liquid-liquid extractive fermentation of lactic acid in a novel semi-partition bioreactor (SPB). J. Biotechnol.

Teke, G.M., 2019. Design and Investigation of a Semi-Partitioned Bioreactor for Continuous Extractive Fermentation. M. Eng thesis.; Stellenbosch University.

Teke, G.M., 2022. Design and Investigation of a Semi-Partitioned Bioreactor (SPB) for Extractive Fermentation using Computational Fluid Dynamic (CFD) simulations and experimental studies. PhD Dissertation; Stellenbosch University.

Van Hecke, W., Kaur, G., De Wever, H., 2014. Advances in-situ product recovery (ISPR) in whole cell biotechnology during the last decade. Biotechnol. Adv. 32, 1245–1255. https://doi.org/10.1016/j.biotechadv.2014.07.003.

Wang, H.Y., 1983. Integrating Biochemical Separation and Purification Steps in Fermentation Processes. Ann. N. Y. Acad. Sci. 413, 313–321.

Wang, X., Li, J., Zhang, L., 2019. Understanding self-accelerated water diffusion within poly-lactic acid via molecular dynamics simulation. Chinese J. Chem. Eng. 27, 759–764. https://doi.org/10.1016/j.cjche.2018.09.009.

Wang, F., Mao, Z.S., 2005. Numerical and experimental investigation of liquid-liquid two-phase flow in stirred tanks. Ind. Eng. Chem. Res. 44, 5776–5787.

Wasewar, K.L., Heesink, A.B.M., Versteeg, G.F., Pangarkar, V.G., 2002. Reactive extraction of lactic acid using alamine 336 in MIBK: Equilibria and kinetics. J. Biotechnol. 97, 59–68.

Weber, B., Schneider, M., Görtz, J., Jupke, A., 2020. Compartment Model for Liquid-Liquid Extraction Columns. Solvent Extr. Ion Exch. 38, 66–87. https://doi.org/10.1080/07366299.2019.1691137.

Yabannavar, V.M., Wang, D.I.C., 1991. Extractive fermentation for lactic acid production. Biotechnol. Bioeng. 37, 1095–1100.

Yao, P.-X., Toda, K., 2008. Lactic acid production in electrodialysis culture. J. Gen. Appl. Microbiol. 36, 111–125.

Young, C.H., Korchinsky, W.J., 1989. Modelling drop-side mass transfer in agitated polydispersed liquid—liquid systems. Chem. Eng. Sci. 44, 2355–2361 https://linkinghub.elsevier.com/retrieve/pii/0009250989851681.